Streamflow response in small upland catchments in the Chilean coastal range to the M_W 8.8 Maule earthquake on 27 February 2010

Christian H. Mohr,[1] David R. Montgomery,[2] Anton Huber,[3] Axel Bronstert,[1] and Andrés Iroumé[4]

Received 3 July 2011; revised 19 April 2012; accepted 24 April 2012; published 5 June 2012.

[1] Hydrological response to earthquakes has long been observed, yet the mechanisms responsible still remain unclear and likely vary in space and time. This study explores the base flow response in small upland catchments of the Coastal Range of south-central Chile after the M_W 8.8 Maule earthquake of 27 February 2010. An initial decline in streamflow followed by an increase of up to 400% of the discharge measured immediately before the earthquake occurred, and diurnal streamflow oscillations intensified after the earthquake. Neither response time, nor time to maximum streamflow discharge showed any relationship with catchment topography or size, suggesting non-uniform release of water across the catchments. The fast response, unaffected stream water temperatures and a simple diffusion model point to the sandy saprolite as the source of the excess water. Base flow recession analysis reveals no evidence for substantial enhancement of lateral hydraulic conductivity in the saprolite after the earthquake. Seismic energy density reached $\sim$170 J/m^3 for the main shock and $\sim$0.9 J/m^3 for the aftershock, exceeding the threshold for liquefaction by undrained consolidation only during the main shock. Although increased hydraulic gradient due to ground acceleration-triggered, undrained consolidation is consistent with empirical magnitude-distance relationships for liquefaction, the lack of independent evidence for liquefaction means that enhanced vertical permeability (probably in combination with co-seismic near-surface dilatancy) cannot be excluded as a potential mechanism. Undrained consolidation may have released additional water from the saturated saprolite into the overlying soil, temporarily reducing water transfer to the creeks but enlarging the cross-section of the saturated zone, which in turn enhanced streamflow after establishment of a new hydraulic equilibrium. The enlarged saturated zone facilitated water uptake by roots and intensified evapotranspiration.

Citation: Mohr, C. H., D. R. Montgomery, A. Huber, A. Bronstert, and A. Iroumé (2012), Streamflow response in small upland catchments in the Chilean coastal range to the M_W 8.8 Maule earthquake on 27 February 2010, *J. Geophys. Res.*, *117*, F02032, doi:10.1029/2011JF002138.

1. Introduction

[2] Hydrological responses to earthquakes include increased streamflow discharge, loss or appearance of springs, changes in subsurface groundwater levels and modifications of hydrochemical properties, like water temperature and water turbidity [*Montgomery and Manga*, 2003; *Roeloffs*, 1996; *Wang and Manga*, 2010a, 2010b]. Co-seismic increases in streamflow discharge can be attributed to the expulsion of water from storage by elastic strain, enhanced hydraulic permeability, changes in the hydraulic head or a combination of these processes. Hence, increased streamflow can be induced by the deformation of aquifers [e.g., *Muir-Wood and King*, 1993; *Roeloffs et al.*, 2003; *Wang et al.*, 2004b] or fractures in the rock strata due to ground acceleration and shaking, resulting in more efficient drainage of the aquifer through enhancement of fracture systems and thereby enhancing groundwater exfiltration rates [e.g., *Briggs*, 1991; *Brodsky et al.*, 2003; *Charmoille et al.*, 2005; *Elkhoury et al.*, 2006; *Rojstaczer et al.*, 1995; *Rojstaczer and Wolf*, 1992; *Tokunaga*, 1999]. *Wang et al.* [2004a] introduced the concept of anisotropic permeability change

[1]Institute of Earth and Environmental Science, University of Potsdam, Potsdam, Germany.
[2]Department of Earth and Space Sciences, University of Washington, Seattle, Washington, USA.
[3]Institute of Geosciences, Universidad Austral de Chile, Valdivia, Chile.
[4]Institute of Forest Management, Universidad Austral de Chile, Valdivia, Chile.

Corresponding author: C. H. Mohr, Institute of Earth and Environmental Science, University of Potsdam, Karl-Liebknecht-Strasse 24-25, D-14476 Potsdam, Germany. (cmohr@uni-potsdam.de)

0148-0227/12/2011JF002138

through which co-seismically enhanced vertical permeability allows a rapid downward draining of groundwater and recharging of the underlying aquifers while the horizontal permeability remains unaffected.

[3] Seismic shaking causes a readjustment of the relative position of clasts and compaction of unconsolidated materials [*Wang et al.*, 2001]. Under undrained conditions, pore water pressure increases and may trigger liquefaction [*Manga*, 2001; *Manga et al.*, 2003; *Montgomery et al.*, 2003; *Wang et al.*, 2001], a process by which the rigidity of saturated deposits is reduced to zero and the sediments become fluid-like, and expels water that, in turn, increases streamflow discharge. Each of these processes has been thought to explain observed co-seismic hydrological response in particular circumstances.

[4] Previous studies reported hydrological responses for meso-scale catchments ($>10^2$ km^2) that produce base flow discharges greater than ~8.5 l/s [e.g., *Montgomery et al.*, 2003]. Catchments of larger spatial extent, however, are mainly composed by heterogeneous geology and topography [e.g., *Wang et al.*, 2004a] which in turn complicate the clear identification of the underlying hydro-seismological processes. In this study, we examine near-surface hydrological response to a high-magnitude earthquake in upland catchments of small spatial extent ($<10^1$ km^2) and homogeneous geological and topographical settings in the Chilean Coastal Range. The small catchment size and relative homogeneity allow exploration of the mechanics controlling earthquake-triggered hydrologic response. We infer from the observed response of small and physiographically comparable headwater catchments that the observed changes in streamflow are likely due to undrained compaction or increased vertical permeability of near-surface material and vertical enlargement of the saturated zone. As the water table rises, the greater cross section of the saturated zone contributes to increased post-seismic subsurface flow toward the creeks.

2. Maule Earthquake and Araucanía Aftershock

[5] The Maule earthquake occurred on 27 February 2010 at 3:34 A.M. local time with a moment magnitude (M_W) of 8.8, the 6th strongest earthquake ever recorded. The hypocenter was located offshore at a depth of 35 km, approximately 105 km north of the City of Concepción (Lat.: 36.4°S, Long.: 73.4°W) [*Vigny et al.*, 2011]. The Maule earthquake was a shallow, thrust-faulting event along the convergent margin where the oceanic Nazca plate subducts beneath continental South America. This event ruptured the Nazca margin over a length of approximately 600 km and closed the Concepción-Constitución or Darwin seismic gap of the Andean subduction zone [*Lorito et al.*, 2011, *Madariaga et al.*, 2010; *Moreno et al.*, 2010; *Sparkes et al.*, 2010]. With a duration of ~150 s it was an extraordinarily long rupture event and the felt intensity reached VIII on the modified Mercalli scale. More than 300 aftershocks of moment magnitude >M_W 5.0 occurred before May 2010, 21 of which exceeded M_W 6.0. The Araucanía earthquake, the most intense aftershock, occurred on 2 January 2011 with a moment magnitude (M_W) of 7.1 (USGS NEIC Catalog, http://earthquake.usgs.gov/earthquakes/eqarchives/epic). The hypocenter was located at a depth of 21 km at the southern end of the aftershock region, about 70 km northwest of the City of Temuco (Lat.: 38.4°S, Long.: 73.3°W). The earthquake lasted for ~20 s and the felt intensity reached VII on the modified Mercalli scale.

3. Study Area and Weather Conditions

[6] Streamflow response to the earthquake was recorded by a network of 10 experimental catchments established in the Chilean coastal range to analyze hydrological and erosional processes of different forest management practices [*Huber et al.*, 2010]. The catchments are located about 500 km south of Santiago, on the eastern slope of the Coastal Range facing the dry central valley between the cities of Concepción and Los Angeles in the Bío-Bío Region, close to the city of Nacimiento (Figure 1). The epicenters of the main earthquake and the aftershock were located ~130 km and ~110 km, respectively, from the study area, which experienced an estimated maximum ground velocity of ~30 cm/s and ~4.0 cm/s, respectively. Maximum ground acceleration at the study sites reached 0.25–0.30 g for the main shock and 0.05–0.10 g for the Araucanía aftershock (USGS NEIC Catalog, http://earthquake.usgs.gov/earthquakes/eqarchives/epic). Geodetic GPS-measurements at approximately 24 km distance revealed westward motion of ~230 cm and vertical settling of ~50 cm at the study sites [*Vigny et al.*, 2011].

[7] The study area is characterized by a subtropical Mediterranean climate. Annual average precipitation is 1150 mm, concentrated between April and September and contributing 95% of the total annual yield. Annual average temperature is 13°C and summer temperature can exceed 40°C, producing high evapotranspiration rates. Although soil water content is low during summer [*Huber et al.*, 2010], soil moisture in the deepest soil layers was high prior the earthquake (Figure 2). According to *Huber et al.* [2010], the deeper soil layers/saprolite becomes saturated when soil moisture comes up to 0.35–0.41 cm^3/cm^3. These values are comparable to typical porosities of sandy clay loam, which can reach ~0.39 cm^3/cm^3 [*Rawls et al.*, 1993]. Moreover, due to the high stone content of lower soil layers (up to 90%) at least a partial saturation of the saprolite layer is expected. According to *Scheffer and Schachtschabel* [2010] only minor capillary rise of some tens of centimeters may be expected in sandy soil texture. Thus, a shallow, and likely perched, groundwater table was likely at about 200 cm depth prior to the earthquake (Figure 2).

[8] The catchments vary from 7.8 to 412.9 ha in size and altitudes range between ~250 and 450 m asl. All catchments are in the uplands and extend up to the ridges of the coastal mountain range. Mean slopes vary from 14 to 22° but exceed 60° along the creeks or road cuts, promoting active gully formation along the road cuts and steep former timber drag lines perpendicular to the creeks. The small size and similar shape and slope among the catchments facilitate inter-catchment comparison [e.g., *Bosch and Hewlett*, 1982], but limit the potential to investigate contrasting catchment properties. The mean stream gradients vary between 10 and 15°. Despite local gradient variations, the stream profiles are mainly straight in shape with minor deviations: stream profiles of catchments 2, 6, and 9 are slightly concave, whereas the stream profiles of catchments 7 and 10 are slightly sigmoidal. The study catchments are drained by a single creek except for catchments 6, 7, 8 and 11 which consist of at least two major tributaries. The length of the principal streams (the longest tributary) varies from 400 m in catchment 2 to

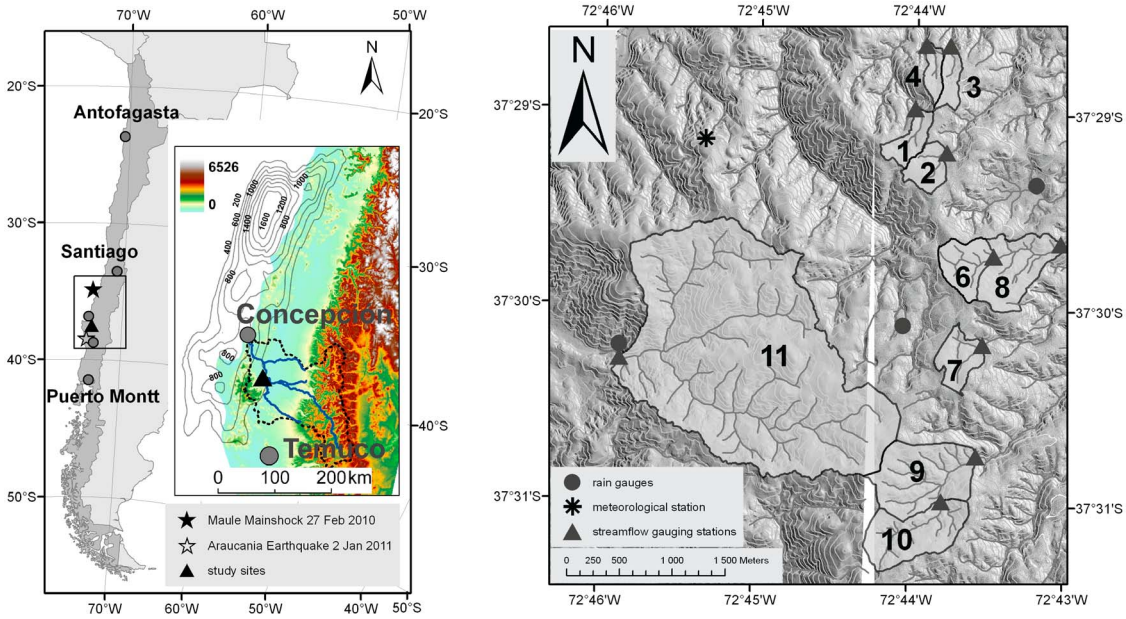

Figure 1. (left) Location of the study area in relation to the epicenters of Maule earthquake (27 February 2010) and the Araucanía Aftershock (2 January 2011). The inset shows the Bío-Bío drainage basin as a dotted line. The contours show the slip in the main shock; the contour interval is 200 cm [*Tong et al.*, 2010]. The representation of the elevation (m asl) is derived from GTOPO30 data (http://demex.cr.usgs.gov/DEMEX/). (right) The location of the monitored catchments showing the positions of the rain gauges, the meteorological station and the streamflow gauging stations. Elevations are derived from a LiDAR DEM and the contour interval is 20 m. The numbers correspond to the following catchments: 1: *Pinus rad.* Control; 2: *Pinus rad.* selective thinning; 3 and 4: Former *Pinus rad.* Plantation, clear-cutting in winter 2009 (3) and summer 2010 (4); 6: *Eucalyptus glob.* regeneration; 7: *Eucalyptus glob.* plantation; 8: Mixed vegetation; 9: Native Forest; 10: Native Forest; 11: Juvenile *Eucalyptus glob.* plantation.

2700 m in catchment 11. Schist bedrock is exposed in the channel beds and alluvial deposits are present only locally. The catchments preferentially face to the north and east and drain toward the Bío-Bío River (Figure 1).

[9] All streams are surrounded by a 7.5–15 m wide planted riparian buffer strips on each side. The buffer strips are composed of dense native brush and deep-rooting trees, including Arrayán (*Luma apiculata DC. Burret*), Boldo (*Peumus boldus Mol.*), Roble (*Nothofagus obliqua Mirb.*) and Lingue (*Persea lingue Nees*). In most cases the buffer strips are restricted to the steep slopes close to the creeks but may also extend into small wetlands, as in the case of catchment 2. The buffers account for 5.6 to 22.6% of total catchment area and are intended to protect the streams from sediment input due to timber harvest of plantations of fast growing and highly water consuming exotic *Pinus radiata D. Don* and *Eucalyptus spp.* Two catchments (No. 9 and 10) are excluded from silvicultural exploitation and retain native forest. The main characteristics of the catchments are summarized in Table 1.

[10] The dominant soil type is a clayey to loamy Luvisol with variable structure on a small scale due to fragments of bedrock within the topsoil, a complex distribution of recent and former root systems, and disturbance by timber harvest. The soil patchiness enhances the variability of hydraulic conductivity and intensifies preferential flow patterns [e.g., *Ziegler et al.*, 2006]. Truncated soil profiles exposing low-conductive B-horizons and evidence of recent incision indicate active soil erosion and landsliding, likely triggered by forest clearing [e.g., *Montgomery et al.*, 2000]. During the first rainy season after the earthquake numerous landslides were observed, mostly concentrated at road cuts. Soil depth typically ranges between 160 and 170 cm but some road cut exposures of soil exceed 250 cm. At its base, the loamy-sandy saprolite can reach depths of 560 $\pm$ 215 cm and overlays homogeneous schist, which forms the geological basement and parental material [*Melnick et al.*, 2009]. Field surveys confirm the saprolite to be a highly permeable layer because subsurface flow has been observed exfiltrating from this layer in road cuts during dry summer months. The near-surface part of the schist is heavily fractured and together with the saprolite forms an unconfined near-surface aquifer. The total depth of the unconsolidated and fractured material locally exceeds 700 cm.

[11] Weather conditions around the time of the Maule earthquake were dry despite an extraordinarily wet February 2010 when 82 mm of rainfall greatly exceeded the long-term monthly average of 7 mm. Two major rainfall events contributed to the greatest part of the February rainfall. The first event occurred 6–7 February and contributed ~60 mm, the second event occurred 17–18 February and contributed ~20 mm. Between 19 February and 5 May 2010 no significant precipitation was recorded. Hence, during this period, the total discharge was contributed by base flow exclusively. Strong transpiration of the vegetation layer during the dry summer months [*Huber et al.*, 2010] governed pre-seismic base flow recession. The last intense rainfall event before the

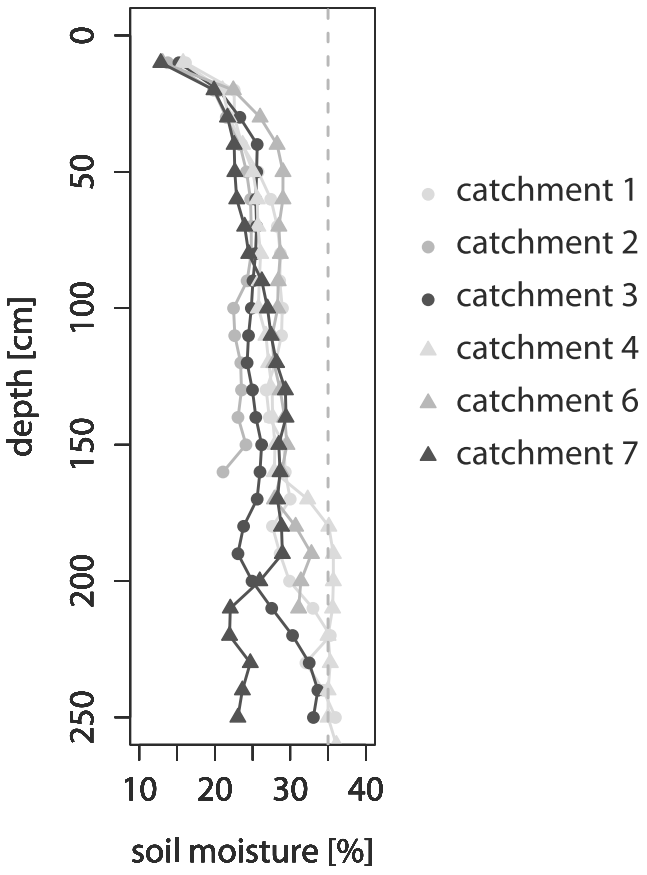

Figure 2. Soil moisture (vol. %) measured along transects of access tubes (n = 6–15) by TRIME-TDR on 19 February 2010. Dashed line represents minimum water content (35%) needed to saturate the saprolite [*Huber et al.*, 2010].

aftershock delivered a total of 23 mm between 10 and 11 December 2010 6 mm of rainfall on 17 December did not generate significant runoff. Total precipitation in December 2010 was 42 mm, well within the long term monthly average.

4. Methods and Data

[12] The streamflow in all catchments was monitored by V notched Thompson-type weirs except for the catchment with the largest spatial extent (No. 11; Pichún grande). Here, discharge was measured by a flume. Water stage was recorded by a custom-built float at a sampling interval of 3 min with an accuracy of 2 mm. For a subset of catchments, the water temperature was measured inside the weirs by Hobo-Pendant water temperature loggers (Hobo Pendant temp., Ref. UA-001-64) with the same temporal resolution (3 min) and an accuracy of ±0.54°C. Precipitation was recorded by three Hobo tipping bucket rainfall gauges distributed over the study area at suitable and accessible sites (Figure 1).

[13] To determine the effect of the earthquake, discharge records were compared for clear differences in streamflow prior to and after the seismic events. In order to minimize the effect of precipitation on total discharge, only base flow as the component of streamflow provided by groundwater was considered [*Manga*, 2001]. Since low pre-seismic base flow discharge has been measured across all catchments, the

Table 1. Main Characteristics of the Experimental Catchments

Catchment	1	2	3	4	6	7	8	9	10	11
Area (ha)	12.65	13.47	9.47	7.76	20.47	17.43	36.51	54.15	41.30	412.90
Landuse	control	selective thinning	clear-cutting winter 09	clear-cutting summer 10	regeneration	plantation	mixed forestry	control	control	Plantation
Vegetation	*Pinus radiata*	*Pinus radiata*	-	-	*Eucalyptus globulus*	*Eucalyptus globulus*	*Eucalyptus glob.* and *Pinus rad.*	Native species	Native species	*Eucalyptus globulus*
Tree-Density (tree/ha)	320	315	-	-	1326	893	-	-	-	-
Plantation age (yr)	24	24	-	-	10	10	24/10[a]	-	-	3
Riparian buffer (ha)	0.83	0.90	1.15	1.0[b]	4.62	0.97	7.42	20.49[c]	19.16[c]	45.30
Altitude (m asl)	328–377	333–367	255–320	246–318	322–366	369–407	259–367	376–476	389–467	320–476
Catchment slope (°)	14.7 ± 8.5	14.2 ± 8.6	18.2 ± 10.2	20.4 ± 10.8	18.4 ± 9.9	15.4 ± 8.8	18.9 ± 9.2	21.6 ± 9.4	19.9 ± 9.1	19.4 ± 10.3
Slope of stream (°)	10.0 ± 7.3	13.0 ± 8.9	15.1 ± 10.7	18.1 ± 10.7	13.2 ± 9.2	9.8 ± 6.9	11.8 ± 9.6	15.2 ± 9.4	13.3 ± 8.8	11.6 ± 9.2
Length of principle stream (m)	497	399	487	466	532	454	1323	1625	921	2694
Max. flow length (m)	762	692	773	711	1284[d]	890[d]	1420[d]	2044	1330	3682
Wetness index	4.76 ± 1.84	4.48 ± 1.08	4.33 ± 1.24	4.00 ± 1.15	4.41 ± 1.17	4.65 ± 1.19	4.34 ± 1.23	4.21 ± 1.17	4.22 ± 1.13	4.15 ± 1.25

[a]24 years *Pinus rad.*, 10 years eucalyptus plantation.
[b]Riparian buffer strip completely logged during clear-cutting in March/April 2010.
[c]Including native vegetation within catchment area.
[d]Drainage system modified by timber roads.

Pichún grande catchment is analyzed in the most detail. This catchment is by far the largest in spatial extent and shows the highest discharge which, in turn, imparts greater accuracy to the discharge measurements. The base flow was determined by the constant slope method, which graphically determines the base flow component of total discharge by connecting the point of initial hydrograph rise with the end of the hydrograph recession of equal discharge prior to the rise by a straight line [e.g., *Blume et al.*, 2007; *Dingman*, 2002]. The response time was estimated for all catchments as the time lag between the earthquake and the first rise in streamflow exceeding the pre-seismic discharge. In order to quantify the effect of the seismic event on streamflow discharge, the maximum percentage change in post-seismic base flow was calculated and the excess water for a subset of catchments was estimated from the difference between the observed discharge and an estimate of what the discharge would have been in the absence of an earthquake [*Manga*, 2001].

[14] Hydraulic conductivity, which can be estimated by the hydrograph recession constant, is a parameter closely related to the geometrical and physical properties of the aquifer. Thus, the recession constant can be used to describe aquifer-scale transient groundwater flow from an unconfined aquifer seeping into a stream [e.g., *Manga*, 2001; *Manga et al.*, 2003; *Montgomery et al.*, 2003]. Although recession analysis only considers isotropic hydraulic permeability [*Wang et al.*, 2004a] and neglects capillary effects, it is a suitable tool to detect catchment-scale, earthquake-caused changes in hydraulic properties [e.g., *Manga et al.*, 2003]. We compared pre- and post-seismic recession constants calculated by the constant k method [*Blume et al.*, 2007]:

$$\delta Q/\delta t = -k \bullet Q(t) \tag{1}$$

which can be rearranged to yield

$$k = -\delta Q/\delta t \bullet 1/Q(t) \tag{2}$$

where k is the recession constant (1/day) and Q (t) is discharge at time t (m^3/day). Due to low base flow discharge was summed up to daily volume, which in turn negatively affects the accuracy of the water stage-discharge relation. Summing up to daily volume makes the recessions smoother since short timescale variations are averaged making the determination of k more reliable.

[15] In order to quantitatively characterize topological properties of the catchments, high-resolution digital terrain models (DTM) based on airborne LiDAR data were analyzed. LiDAR is able to penetrate dense vegetation cover which makes it an accurate tool for surface analysis under forest canopy [*Reutebuch et al.*, 2003]. The surface analysis was achieved with ArcGIS or SAGA-GIS. All hydrological calculations were done with the statistical software R.

5. Approach

[16] After the earthquake, a strong increase of streamflow discharge—the most striking hydrological response to the earthquake—was preceded by an immediate but transient drop of streamflow. Infiltration excess overland flow and saturation overland flow are not possible sources of the increased post-seismic flow because there was no rainfall for several days prior to the earthquake. The observed streamflow in the experimental catchments during the study period originated from groundwater sources as exfiltrating groundwater flow or return flow. Groundwater flux is governed by the hydraulic gradient $\delta h/\delta l$ of the groundwater (δh corresponds to the difference in hydraulic head over the length of the flow path δl) and the hydraulic conductivity kf of the aquifer releasing water into the creek, which can be described by the Darcy-equation:

$$Q = vD \bullet A = kf \bullet \delta h/\delta l \bullet A \tag{3}$$

where Q is discharge, vD is the Darcy-velocity (filter velocity) and A is the cross section of the aquifer perpendicular to the flow direction. Substituting the product of the aquifer height H and the specific aquifer width (or unit width) w for A yields:

$$Q = kf \bullet \delta h/\delta l \bullet H \bullet w \tag{4}$$

According to equation (4), a rise in groundwater exfiltration would take place if at least one of the variables or terms of that equation increases. Neither the unit aquifer width w nor the aquifer height H can directly change as a result of the earthquake because the catchments are restricted to the upland headwaters. Considering the topographical position of the catchments, no higher elevated regions are present in the vicinity. Thus, there is no possibility of additional groundwater being released from an elevated hinterland, e.g., the Andes Mountains, recharging the local groundwater of the catchments by an elevated hydraulic head from outside the topographically defined drainage basin. Hence, the observed hydrological response to the earthquake was a result of autochthonous changes in either hydraulic conductivity kf and/or the hydraulic gradient $\delta h/\delta l$ within the catchments.

6. Observations and Results

[17] The hydrographs of all study catchments showed streamflow response immediately after the earthquake (Figures 3 and 4). The hydrological responses showed similar but not uniform patterns among the catchments. Most of the catchments (6 out of 10) experienced an immediate drop in discharge within the first 3 min of sampling after the earthquake, followed by a large increase in streamflow. A summary of the streamflow responses of each catchment is shown in Table 2.

[18] In quantitative terms, the increase in the mean base flow after the earthquake is the most striking hydrological signal. In contrast to the widely reported increase in streamflow [e.g., *Manga et al.*, 2003; *Montgomery and Manga*, 2003; *Muir-Wood and King*, 1993; *Rojstaczer et al.*, 1995] an initial decline in streamflow is reported rarely [*Rojstaczer and Wolf*, 1992; *Tertulliani and Cucci*, 2009]. In all of the study catchments, the magnitude of post-seismic streamflow increase greatly exceeded the co-seismic drop. With a reaction time of 15 min to up to 3 h, the observed increases ranged between 110–400 percent of the base flow registered immediately prior to the earthquake. The time to post-seismic peak discharge varied between 5 and 6 h (catchments No. 2 and 8) to more than 4 days (catchments No. 6, 7 and 9; see Table 2).

[19] After reaching the post-seismic maximum discharge, the discharge receded gradually in most catchments. In some

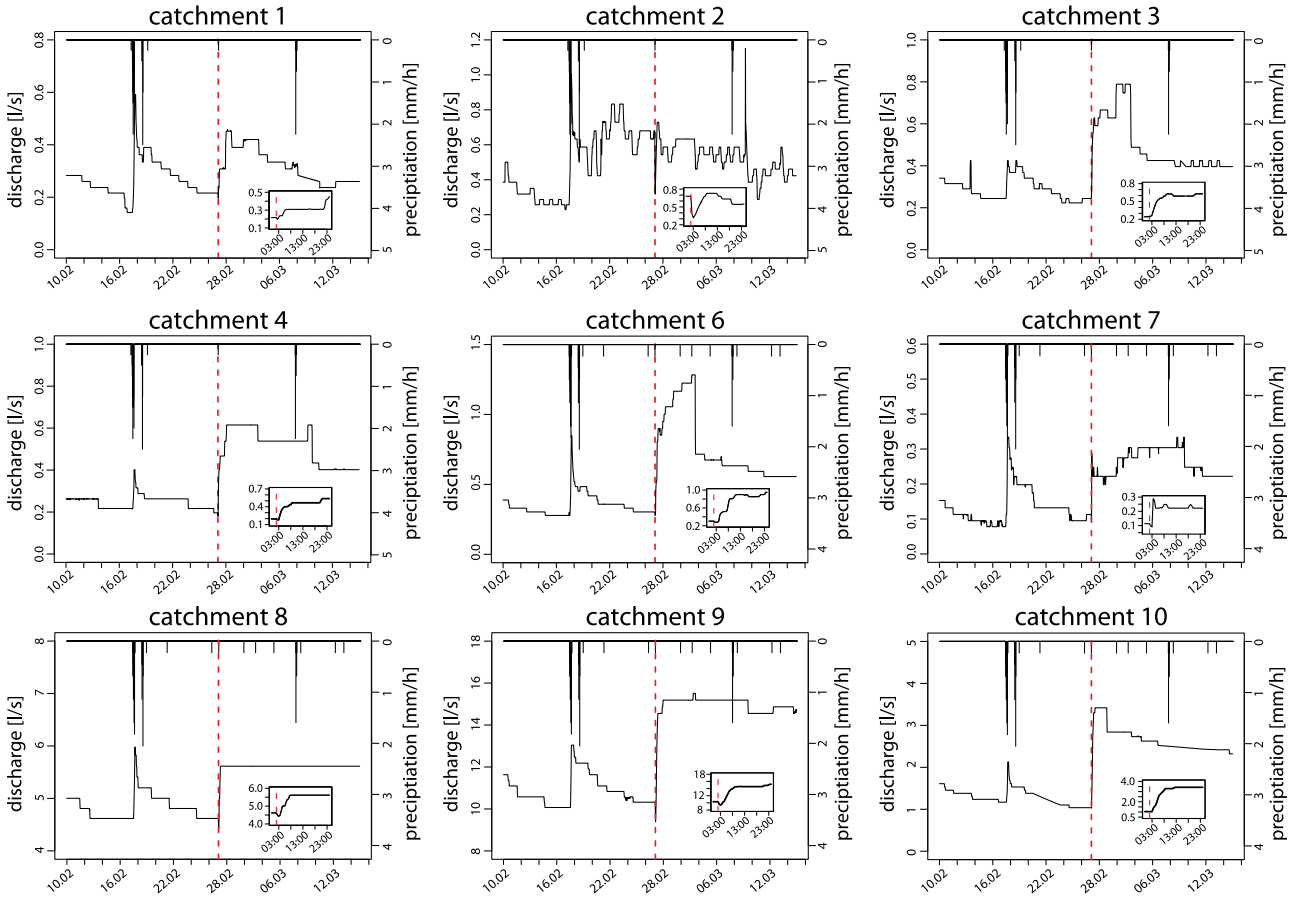

Figure 3. Hydrographs of the catchments showing the hydrological response of the 9 smaller catchments to the earthquake. The small inset figures show in greater detail the immediate co-seismic decline of streamflow discharge on 27 February 2010. The dotted red lines represent the earthquake.

catchments (e.g., catchments No. 3 and 6), the slope of the post-seismic decrease in streamflow was comparable to the steep increase. Despite substantial scatter, pre- and post-seismic recession constants do not exhibit a consistent change, as shown by the overlap of error bars with the 1:1-line (Figure 5). Statistical tests only showed a significant decrease in catchment No. 11 while some recession constants in catchments No. 2, 3, 4, 8, and 11 slightly decreased and others increased (catchments No. 1, 7). A linear model fit with 1000 bootstrapped samples yielded the following model:

$$k_{post} = 1.02 \bullet k_{pre} + 0.03 \quad (5)$$

where k_{kpost} is the recession constant k after the earthquake and k_{pre} prior to the earthquake. Although the standard deviations for both the slope and intercept are considerable (0.51 and 0.09, respectively), pre and post seismic k do not show significant differences.

[20] Diurnal oscillations in streamflow like those observed in catchment 11 are commonly reported and are directly related to evapotranspiration and the replenishment of depleted groundwater storage [*Gribovszki et al.*, 2010]. An increase in the magnitude of the diurnal oscillations is observed in Pichún (No. 11) immediately after the earthquake (Figure 4). Here, the magnitude of diurnal oscillation is defined as the difference between daily maximum and minimum discharge ($Q_{max} - Q_{min}$). The oscillation in Pichún increased from <1.0 l/s prior to the earthquake to 4–5 l/s for the first days after post-seismic peak streamflow on 28 February. Daily maximum discharge occurred in the early mornings and minimum discharge in late afternoons. The observed intensification contrasts with the general trend of declining magnitude of diurnal oscillations starting in December 2009. Diurnal discharge oscillations returned to pre-seismic conditions (<1 l/s) at the end of March 2010.

[21] Catchment No. 2 is a special case since its stream crosses a small wetland directly upslope of the weir. In this catchment, the co-seismic decline of streamflow is highest, decreasing to less than half the pre-seismic discharge and continuing for about 5 h. The magnitude of the diurnal oscillations of between 0.1 and 0.2 l/s remained unaffected by the earthquake. Only on 27 February was the magnitude significantly higher (0.4 l/s) as a result of the strong initial co-seismic decline.

[22] Alterations of streamflow temperature may provide deeper insights into the mechanisms of hydrological response [e.g., *Manga and Rowland*, 2009]. In this study, however, air temperature did not remain stable but varied around the time of the earthquake. That this affected the stream water temperature is evident in the close link between air and water temperatures and the pronounced diurnal temperature cycles during the period from 25 February to 1 March (Figure 6).

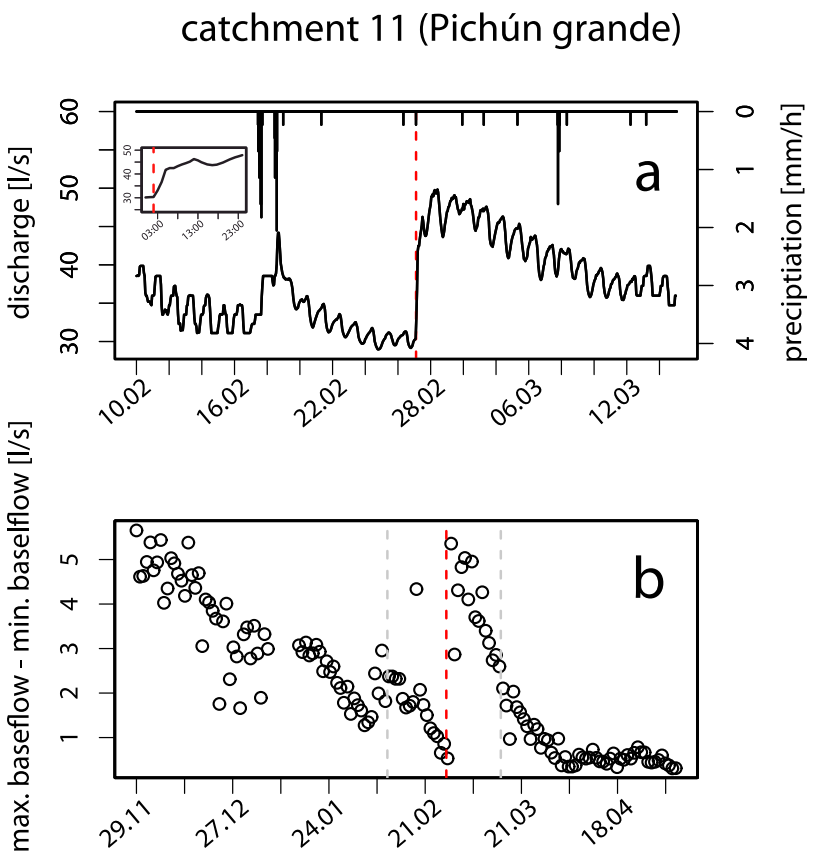

Figure 4. (a) Hydrograph of Pichún grande (catchment No. 11) showing the post-seismic increase in streamflow. The small inset figure shows in greater detail the immediate co-seismic response of streamflow discharge on 27 February 2010. (b) Difference between daily maximum and minimum base flow discharge (l/s) for Pichún grande (catchment No. 11) during the period from 29 November 2009 to 25 April 2010. The dotted gray lines indicate the time period shown in Figure 4a. The dotted red lines represent the earthquake.

[23] Heat flow provides information on tectonic processes while groundwater flow may affect subsurface temperature [*Wang et al.*, 2012]. Hence, changes in groundwater or stream water may be useful to decipher hydro-tectonic processes.

[24] The average increase of all stream temperatures was 0.5 ± 0.1°C during a period of 10 days prior and 10 days after the earthquake, while air temperature increased by 1.6°C from 14.6 ± 1.3°C to 16.2 ± 1.8°C. Maximum mean air temperatures reached 17.8 and 18.8°C on 27–28 February 2010, exceeding pre-seismic average temperatures by 3.2 and 4.2°C and post-seismic temperatures by 1.6 and 2.6°C. On 27 February stream water temperatures of all catchments exceeded average pre-seismic temperatures. The water temperatures registered in all catchments on 28 February exceeded both the average pre- and post-seismic average temperatures (see Table 2). Hence, it is not surprising that the significant post-seismic increase of streamflow temperature observed in all catchments tracked air temperature.

[25] The Araucanía aftershock on 2 January 2011 caused neither an increase or initial decline in streamflow discharge nor a change in streamflow temperature in any of the study catchments (Figure 7).

[26] The observed response of the study catchments can be summarized as an immediate co-seismic decline in streamflow continuing for a period of up to 2 h, followed by a significant increase in base flow (~110–400%) within a response time of 15 min to 3 h, accompanied by an increase in the diurnal oscillation by up to one order of magnitude for a period of 30 days. No discernible change in either streamflow temperature or recession constants was associated with the earthquake.

[27] Although similarities in the hydrological response indicate similarity of the underlying processes, variable duration and magnitude of excess flow or differences in response time also reflect differences in hydro-geomorphic properties among the catchments. First- and second-order topographical indices (mean catchment slope, Gravelius compactness index), average wetness index and stream properties (length, average gradient and shape) were all correlated to the magnitude of increase in streamflow discharge, reaction time of the hydrological response and time to post-seismic peak streamflow discharge (Table 3) [see *Wilson and Gallant*, 2000]. The Gravelius compactness index describes the ratio between the perimeter of a catchment and the perimeter of a circle with the same area. This index is only suitable for inter-basin comparison of the same spatial scales [*Bárdossy and Schmidt*, 2002], as is the case here. Stream lengths were calculated by threshold contributing area of 2 ha, which corresponds to channel head locations determined from field observations and GPS.

[28] Hydrological variables like co-seismic discharge or minimum and maximum post-seismic discharge were also

Table 2. Summary of Hydrological Responses to the Maule Earthquake in the Experimental Catchments[a]

Catchment	1	2	3	4	6	7	8	9	10	11
$Q_{coseismic}$ (l/s)	0.22	0.68	0.24	0.20	0.30	0.11	4.62	10.32	1.04	30.32
Min. $Q_{post\text{-}seismic}$ (l/s)	0.19	0.32	-	0.18	0.28	0.10	4.46	9.4	1.03	-
Max. $Q_{post\text{-}seismic}$ (l/s)	0.46	0.73	0.79	0.62	1.28	0.33	5.61	15.51	3.42	49.83
Increase (%)	210	110	330	310	430	300	120	150	330	160
Response time (min)	47	179	20	60	113	56	101	101	50	15
Time of max. $Q_{post\text{-}seismic}$ (date + time)	2010-02-28 03:30	2010-02-27 09:00	2010-03-01 22:00	2010-02-28 02:00	2010-03-03 06:00	2010-03-03 09:30	2010-02-27 08:00	2010-03-03 09:00	2010-02-27 12:30	2010-02-28 01:00
Pre-seismic stream temperature (°C)	13.9 ± 0.1	-	13.7 ± 0.2	14.1 ± 0.2	12.7 ± 0.1	-	13.2 ± 0.2	12.5 ± 0.1	12.9 ± 0.2	-
Post-seismic stream temperature (°C)	14.3 ± 0.2*	-	14.4 ± 0.4*	14.7 ± 0.4*	13.2 ± 0.2*	-	13.7 ± 0.3*	13.0 ± 0.3*	13.3 ± 0.3*	-
Stream temperature (°C) 27 February	14.1	-	14.3	14.8	13.0	-	13.6	12.9	13.3	-
Stream temperature 28 February	14.6	-	15.2	15.5	13.4	-	14.1	13.6	16.7	-

[a] $Q_{co\text{-}seismic}$ is defined as the streamflow discharge registered immediately before the earthquake (3.34 A.M. local time.), min. $Q_{post\text{-}seismic}$ refers to the minimal streamflow discharge measured during the initial decline after the earthquake and max. $Q_{post\text{-}seismic}$ to the maximum streamflow discharge registered after the earthquake (ignoring runoff response to rainfall events). Daily mean water temperatures (in °C) are given for 10 days pre- and post-seismic periods. Pre-seismic period continued from 17 February 2010 to 26 February 2010 and post-earthquake period from 27 February 2010 to 8 March 2010. Change of temperatures after the earthquake was tested by using the Kruskal-Wallis test and differences were taken to be significant with $p < 0.05$. Significant differences are indicated by the asterisk.

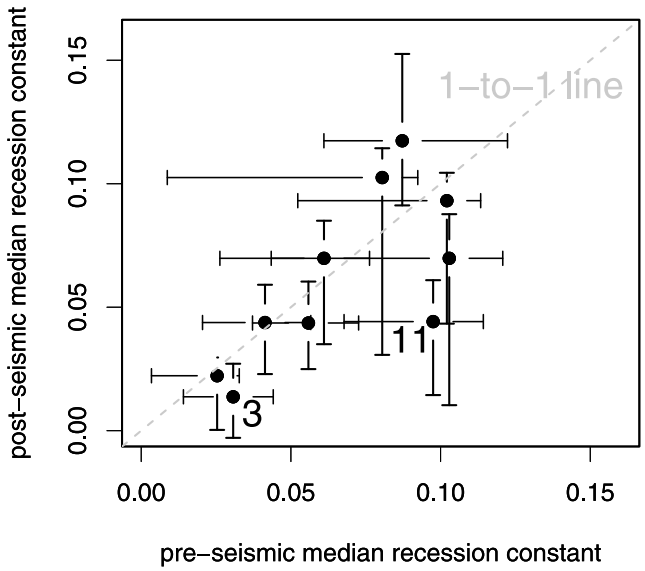

Figure 5. Pre-seismic versus post-seismic recession constants, calculated as daily values (m^3/day) for all catchments. Numbers refer to catchment numeration. The pre-earthquake period continued from 17 April 2008 to 26 February 2010. For post-earthquake recession constants, the period from 27 February 2010 to 12 July 2010 was considered. Error bars show range of values for individual rainfall events. Recession constants were calculated with the R-package Tiger (D. Reusser, Tiger: Time Series of Grouped Errors, unpublished data, 2010, http://cran.r-project.org/web/packages/tiger).

considered in the correlation analysis. Due to small sample size ($n = 10$) and non-normal distribution, bootstrapping was performed to assess accuracy in statistical analyses. Bootstrapping is a simple resampling technique and involves choosing and analyzing random samples with replacement from the same data set. This means that each sample is selected separately and randomly from the original data set and a particular sample from this data set could appear multiple times in the bootstrap sample. Increasing the number of samples may reduce the effects of random sampling errors but cannot augment the information content of the original data. Bootstrapping may be used for estimating the statistics in the case of small sample size or unknown distribution because it measures these statistics when sampling from an approximating distribution. Based on such sampling repeated 1000 times, the strongest correlation has been found between post-seismic streamflow increase and co-seismic discharge, post-seismic maximum and minimum streamflow discharge. All of these variables, in turn, exhibit correlation to the scaling variables of catchment size, stream length, longest flow path and catchment perimeter. These results are similar to the observations of *Montgomery et al.* [2003]. Topographical indices and stream properties (mean stream slope, mean catchment slope and mean topographical wetness index (TWI) as a function of slope are uncorrelated with streamflow increase, response time or time to post-seismic peak streamflow discharge. Both response time and time to post-seismic streamflow increase are not correlated to any topographical index, with a correlation coefficient

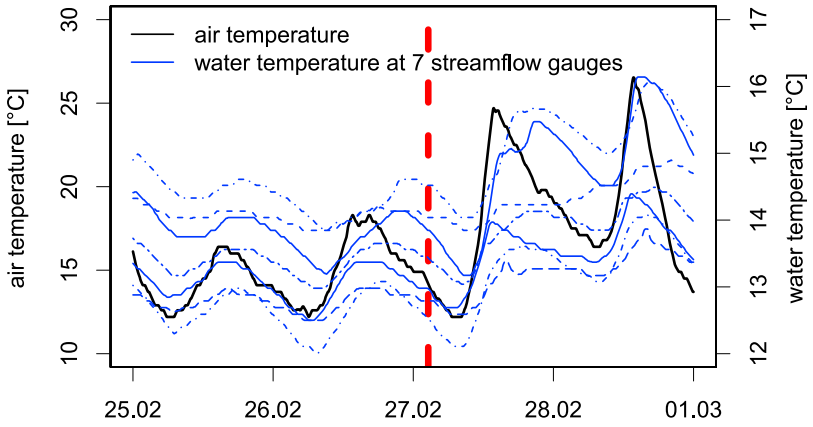

Figure 6. Water temperature at streamflow gauges of catchments 1, 3, 4, 6, 8, 9 and 10 and air temperature recorded at the meteorological station for the period from 25 February 2010 to 1 March 2010. Water temperature is represented by blue lines and air temperature by the black line, both smoothed by a 60-min running mean filter. The time of the earthquake is marked by the red dashed line.

only reaching −0.41 for the catchment size and Gravelius compactness index (Table 3).

7. Discussion

[29] The observed pattern of hydrological response constrains possible mechanisms for the source of the excess water.

7.1. Where Does the Excess Water Come From?

[30] Due to the high evapotranspiration rates of the exotic plantations and juvenile native forest, streamflow decreased continuously during the dry season. The small volume of streamflow makes the water temperature more susceptible to variations in air temperature due to facilitated heat exchange with the land and/or atmosphere [*Manga and Rowland*, 2009]. The close relationship between water and air temperature can be seen in their similar dynamics (Figure 6) and their relationship remained unaffected by the earthquake. Expanding the analysis to a longer period of time (16 February–10 March), no substantial temperature changes before and after the earthquake have been observed which cannot be explained by air temperature variations (Figure 8). *Manga and Rowland*

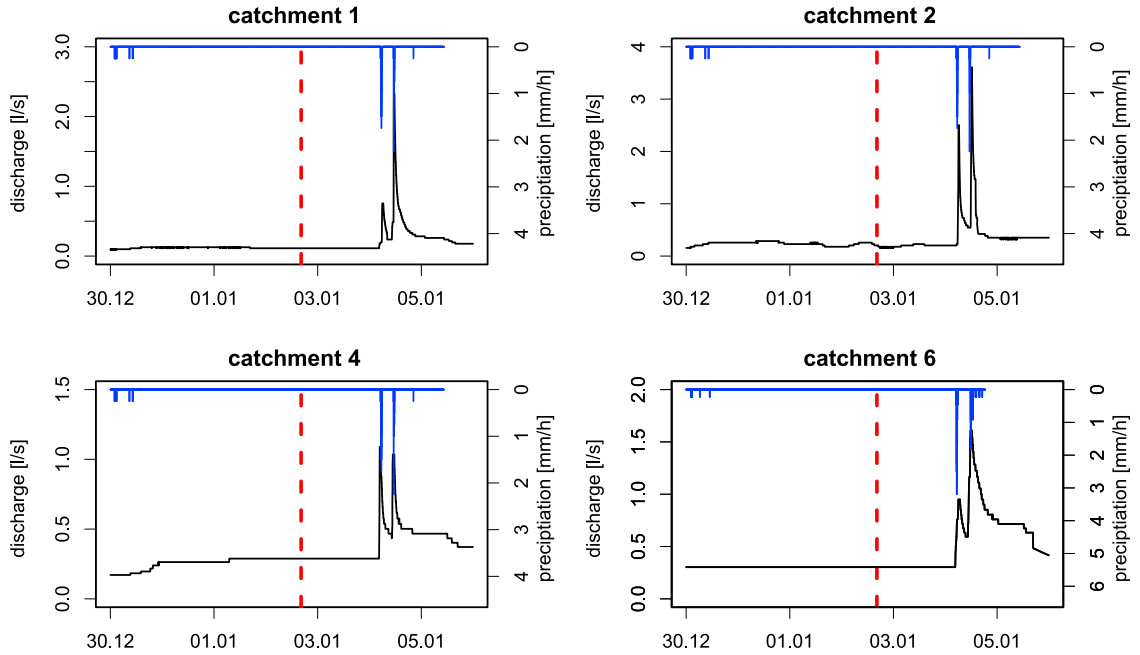

Figure 7. Hydrographs showing no hydrological response to the Araucanía aftershock in the streamflow. The time of the aftershock is indicated by the dashed red line. Here, only catchments No. 1, 2, 4 and 6 are presented for the period of 31 December 2010 to 6 January 2011 as representative examples; none of the monitored catchments showed any hydrological response to the aftershock.

Table 3. Median Correlation Coefficients Based on 1000 Bootstrapped Samples[a]

	Post-Seismic Increase of Streamflow Discharge	Response Time	Time to Post-Seismic Peak Streamflow Discharge
Post-seismic increase of streamflow discharge	1.00	−0.40	−0.02
Response time	−0.40	1.00	−0.08
Time to post-seismic peak streamflow discharge	−0.02	−0.08	1.00
Co-seismic streamflow discharge	0.99	−0.31	−0.03
Minimum post-seismic streamflow discharge	0.99	−0.34	−0.07
Maximum post-seismic streamflow discharge	0.99	−0.34	−0.05
Mean slope of stream	−0.08	0.08	0.05
Mean catchment slope	0.44	−0.29	0.14
TWI	−0.46	0.15	0.15
Gravelius Index	−0.30	−0.41	−0.31
Stream length	0.94	−0.29	−0.05
Catchment area	0.99	−0.41	−0.11
Perimeter	0.97	−0.36	−0.15
Longest flowpath	0.97	−0.27	0.05

[a]Co-seismic streamflow discharge, minimum and maximum post-seismic discharge and post-seismic increase in streamflow discharge are considered in l/s, response time and time to post-seismic peak streamflow discharge in minutes after the earthquake, stream and catchment slopes in degree (°), catchment area in hectares and stream length, perimeter and longest flow path in meters. Gravelius Index and TWI (Topographical Wetness Index) are dimensionless.

[2009] attribute unaffected temperatures of pre- and post-seismic waters to a common near-surface source.

[31] Mid-crustal fault displacement processes that expel fluids generally result in increased water temperature [*Nakamura and Wakita*, 1984; *Rojstaczer et al.*, 1995; *Sato et al.*, 1992; *Wang and Manga*, 2010a], whereas a decrease in water temperature may be related to increased groundwater recharge induced by earthquake-enhanced vertical permeability [*Wang et al.*, 2012]. Although the accuracy of streamflow temperature measurement is limited, and may not capture millidegree scale response, our water temperature measurements support a shallow source for the observed earthquake-induced streamflow variations.

[32] A shallow source is also indicated by incorporating observed hydrologic response times into the relationship derived by *Roeloffs* [1996] to estimate the source depth:

$$z = \sqrt{\frac{T \bullet D}{11}} \tag{6}$$

where z is depth below the water table in meters, D the hydraulic diffusivity (m^2/s) and T the time scale of pore pressure dissipation to the water table in seconds. For a typical diffusivity of fine sand (such as the coarsest grain size fraction of the loamy soil covering the saprolite) [$\sim 10^{-1}$ m^2/s,

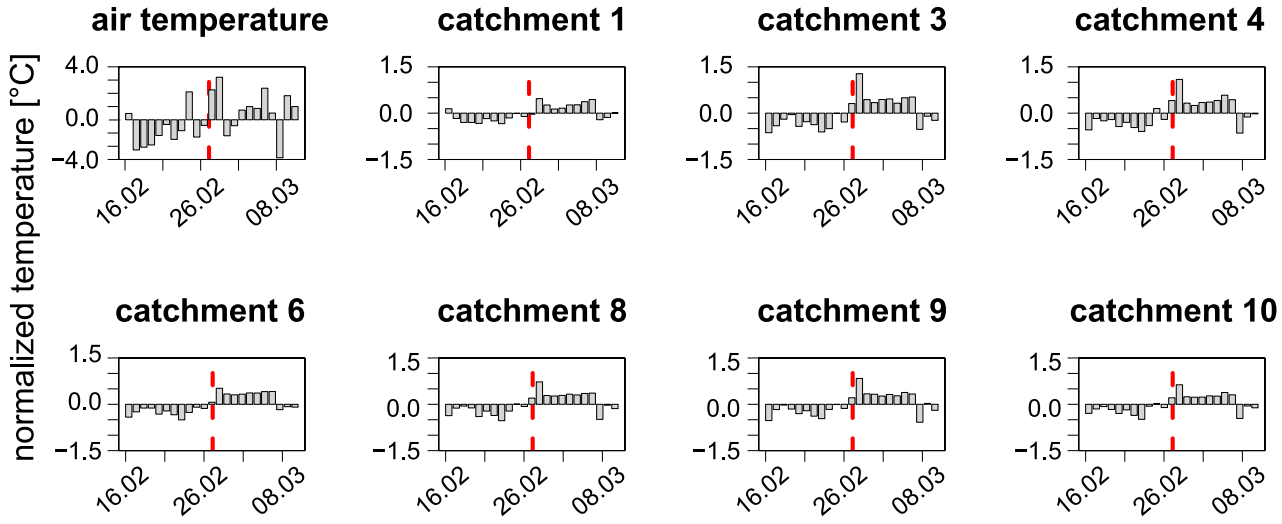

Figure 8. Daily mean water and air temperatures (°C) for the period from 16 February 2010 to 10 March 2010 normalized to the corresponding mean temperature over that period. Although some differences between pre- and post-seismic water temperatures are apparent, they remain coupled to air temperature throughout the measurement period. The time of the earthquake is highlighted by the dashed red lines.

Roeloffs, 1996] the response times of 15 min to 3 h indicate a maximum depth of $\sim 6 \pm 2.1$ m averaged over all catchments. This depth is consistent with the saprolite-bedrock-interface.

[33] Assuming a source of the water equally distributed across the catchment, the response time and time to peak discharge are expected to be related to drainage area, its related features (e.g., longest flowpath), and its shape (e.g., compactness) among catchments with comparable conditions in soil, geology, topography and land use [*Dingman*, 2002]. Hence, under these conditions, time to peak runoff or response time are expected to show a relationship with catchment size [e.g., *Montgomery and Dietrich*, 2002]. However, this is not the case (see Table 3) and thus an equally distributed source of the excess water is unlikely. Consequently, we infer that the excess water has been released from patchy sources across the catchments.

[34] The fast streamflow response indicates sources located close-by the creeks since proximity of the source area to the creeks facilitates a fast response at the catchment outlet (see Tables 2 and 3, *Dingman*, 2002). A strong correlation between the magnitude of the post-seismic increase and the stream length supports this assumption. Catchment size is also strongly correlated to the magnitude of the post-seismic increase and confirms the importance of catchment scale on the magnitude of the post-seismic increase, similar to the findings of *Montgomery et al.* [2003] for streamflow response to the Nisqually earthquake.

7.2. Increase in Streamflow Discharge by Enhanced Permeability?

[35] Discharge is directly related to hydraulic conductivity (equation (3)) and reflects an integrated response over the whole catchment [e.g., *Ebel et al.*, 2008; *Montgomery and Dietrich*, 2002]. The similar pre- and post-earthquake recession constants show that the lateral hydraulic conductivity has not experienced any consistent enhancement among the catchments (Figure 5), comparable to findings of *Manga* [2001], *Manga et al.* [2003] and *Montgomery et al.* [2003]. Consequently, any seismically induced increase in lateral hydraulic conductivity was minor and/or spatially limited, and failed to enhance substantially the lateral hydraulic conductivity on a catchment scale. Hence, neither seismically induced fracturing as proposed by *Briggs* [1991], *Rojstaczer et al.* [1995] and *Rojstaczer and Wolf* [1992] nor dislodging of obstacles from fractures due to dynamic strain [*Elkhoury et al.*, 2006; *Mogi et al.*, 1989; *Roelofts*, 1998] are a suitable explanation for the observed post-seismic streamflow increase. Dynamic ground shaking might have additionally fractured the topmost schist and thereby enhanced permeability locally. However, streamflow generation by subsurface stormflow is controlled by the most permeable layer (here, the saprolite) where no consistent increase of hydraulic conductivity occurred averaged across the catchment. Hence, possible effects of a slight increase in the permeability of the topmost schist layer are likely masked by the high permeability of the overlying saprolite as streamflow recession analysis would only reveal the hydraulic conductivity of the saprolite. Nevertheless, some additional water might have been expelled from the fissures into the saprolite.

[36] Enhanced lateral permeability may increase streamflow discharge (see equation (3)) but is inconsistent with the observation of an initial streamflow decrease. However, changes of vertical permeability cannot be detected by recession analysis. *Wang et al.* [2004a] reported that topographical position influenced the decrease or increase of streamflow discharge for the Chi-Chi earthquake in Taiwan. Under the force of gravity, unconfined groundwater flows from elevated areas to lower areas. Consequently, upland areas – such as the headwaters in the mountainous region reported here – are typically assumed to be recharge areas while lowlands or downriver valleys are considered as discharge areas [e.g., *Dingman*, 2002] Under these assumptions, an enhancement of vertical permeability causes a drop of the groundwater table in the mountainous terrain and an increase in streamflow in the lower-elevation discharge area where the released groundwater exfiltrates. The Chi-Chi study covered catchments of 10^3 km^2 spatial extent with extensive networks of tributaries in mountainous regions up to 4000 m asl in the Central Range, which is made of metamorphic rocks of various grades whereas the foothills are composed of folded and faulted sandstone and shale. Under pre-earthquake conditions, the vertical permeability has been impeded due to impervious layers promoting lateral flow. During the earthquake, the vertical permeability increased through the formation of subvertical cracks in the sedimentary foothills which in turn enhanced the recharge of the underlying aquifers. As a result enhanced streamflow discharge in the lower area has been recorded [*Wang et al.*, 2004a]. Similar observations were also reported by *Tokunaga* [1999] and *Rojstaczer et al.* [1995] after the Kobe and Loma Prieta Earthquakes. In contrast to the highly differentiated geological setting and topographical gradient of the Chi-Chi study, the small headwater catchments reported here are restricted to mountainous terrain and do not extend to the larger-scale regional discharge areas of the foothills or lowlands. Nevertheless, local discharge is evidenced by perennial streamflow even during long-lasting dry summer periods which in turn are fed by groundwater recharge such as along the catchment crests.

[37] Dilatancy describes the expansion of a material in response to shear and through which its volume increases by loosening up its structure due to the propagation of cracks. Although dilitant microcracks, preferentially oriented parallel to the direction of main stress, increase the porosity [*Scholz*, 2010], pore water redistribution and groundwater transmission could temporarily lower hydraulic head and cause an initial but transient drop in streamflow discharge, as touched on by *Wang et al.* [2001] for the Chi-Chi alluvial fan. This conflicts with the transient increase of hydraulic head caused by undrained consolidation. The dilitant (subvertical?) microcracks, in turn, may have provoked greater vertical permeability resulting in a post-seismic streamflow discharge. Although recession analysis [*Blume et al.*, 2007] allows us to reject substantial changes in lateral groundwater movement, we cannot dismiss vertical permeability enhancement.

7.3. Increase in Streamflow Discharge by Dynamic Strain?

[38] Assuming unchanged aquifer geometry, equation (4) shows that the hydraulic gradient $\delta h/\delta l$ has to change if hydraulic conductivity remains unchanged. Ground shaking

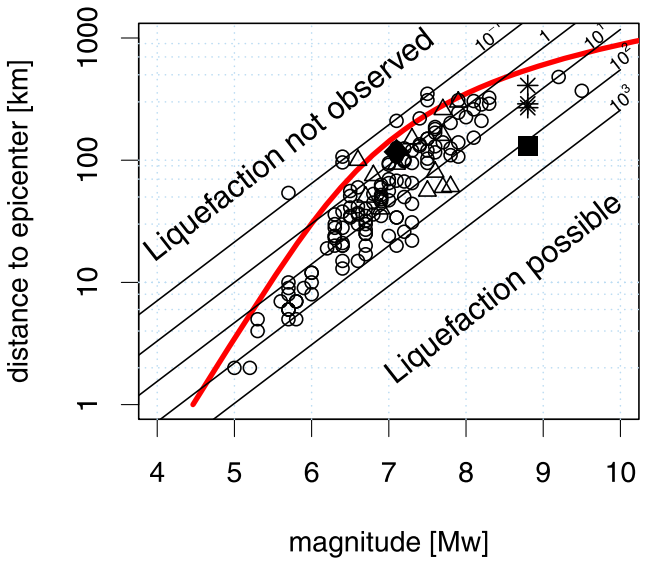

Figure 9. Distance from epicenter versus earthquake magnitude for locations with seismically induced streamflow increase. Circles and triangles represent data compiled by *Wang and Manga* [2010a]. Red line represents the empirical relationship to describe observed liquefaction as a function of earthquake magnitude and distance to epicenter [*Papadopoulos and Lefkopoulos*, 1993]. Inclined lines represent seismic energy density from 10^{-1} to 10^{3} J/m^3 [*Wang and Manga*, 2010b]. Black square represents Maule earthquake and the black diamond the Araucanía aftershock in the studied catchments. Asterisks represent observed streamflow increase during the Maule earthquake in three other catchments in southern Chile.

increases dynamic strain and may cause compaction of undrained saturated near-surface sediments or soils, causing liquefaction that transiently releases water to streams due to closer packing of the sediments [*Manga*, 2001; *Manga et al.*, 2003; *Montgomery et al.*, 2003; *Wang et al.*, 2001]. The maximum distance from epicenters where liquefaction has been observed may be expressed as an empirical function of earthquake magnitude [*Papadopoulos and Lefkopoulos*, 1993]:

$$M = -44 + 3 \bullet 10^{-8} Re + 0.98 \log\ Re \qquad (7)$$

where M is earthquake moment Magnitude (M_W) and Re the maximum epicentral distance in km. All the study catchments lie within this range for the Maule and Araucanía event (Figure 9). Although the observed hydrologic response is consistent with this global data set for liquefaction-induced streamflow increases, this does not necessarily mean that liquefaction is indeed the mechanism for the observed response. M and Re are useful parameters for comparing and relating hydrological responses. However, a single physically based and quantifiable parameter such as the seismic energy density is more suitable. *Wang and Manga* [2010b] define seismic energy density (the summation of ground motion over all relevant modes) as the "maximum seismic energy available in a unit volume to do work on sediment or rock." They empirically define a seismic energy density threshold for triggering liquefaction based data from southern California:

$$\log r = 0.48\ M - 0.33 \log e - 1.4 \qquad (8)$$

where r is the actual epicentral distance in km and e refers to the seismic energy density (J/m^3) [*Wang and Manga*, 2010b]. In addition, laboratory experiments support the field-based evidence for the occurrence of a liquefaction threshold driven by undrained consolidation [*Wang and Manga*, 2010a].

[39] According to *Wang and Manga* [2010b], a minimum seismic energy density of 10^{-3} J/m^3 is required to initiate groundwater level changes but a minimum of 0.1 J/m^3 is necessary to initiate liquefaction. Liquefaction by undrained consolidation is reported to be limited by a required seismic energy density of 30 J/m^3 which in turn closely corresponds to the near-field boundary within one rupture length of the epicenter [*Wang*, 2007; *Wang and Manga*, 2010a]. Thus, undrained consolidation may cause liquefaction-induced streamflow increase only in the near-field. As Figure 1 shows, all catchments lie within the rupture zone. Hence, under suitable geologic and hydrologic conditions, liquefaction by undrained consolidation may be expected for the catchments. Across all catchments, the mean estimated seismic energy density reached 168.2 $\pm$ 5.6 J/m^3 for the main shock, more than 5 times greater than the initiation threshold for liquefaction by undrained consolidation. Even though the epicentral distance is smaller for the Araucanía aftershock ($\sim$110 km), the maximum seismic energy density of 0.9 $\pm$ 0.4 J/m^3 during the aftershock was less than a tenth of that required to initiate liquefaction by this mechanism (see *Wang* [2007] for discussion of liquefaction mechanisms beyond the near-field).

[40] Liquefaction susceptibility is closely related to water content and the sensitivity for sediments to consolidate [e.g., *Wang*, 2007; *Wang and Chia*, 2008; *Wang and Manga*, 2010a]. Nevertheless, the similar post-seismic recession constants do not indicate significant consolidation (equation (5)). Although a liquefaction-triggered streamflow increase by undrained consolidation is possible, field evidence for liquefaction, e.g., conic sand craters, boils or cracks [e.g., *Papadopoulos and Lefkopoulos*, 1993; *Wang and Manga*, 2010a], is lacking.

[41] Liquefaction is a consequence of pore pressure increase when sediments consolidate in 'undrained' conditions during earthquakes [*Wang and Manga*, 2012]. Although undrained consolidation generally requires a confined saturated layer, which is not the case for the saturated saprolite, *Wang and Manga* [2010a] argued that transient pore pressures can increase under unconfined conditions if the duration of seismic shaking is relatively short compared to the time required to dissipate pore pressure in the unconsolidated sediment. Yet, the Maule event continued extraordinarily long. Nevertheless, complete liquefaction of the unconsolidated saprolite into a fluid-like substance is not required to explain the streamflow increase since a near-subsurface fluid pressure rise is sufficient.

[42] As reported by *Carrigan et al.* [1991], volumetric strain enhances horizontal groundwater flow, but also

elevates the water table into the unsaturated zone. The rise, however, is limited by the volume of the water which had been mobilized by undrained compaction which, in turn, decreased the porosity [*Manga*, 2001; *Wang et al.*, 2001]. Thus, undrained consolidation of the sandy saprolite would force water in a patchy pattern to rise upward toward the water table [*Lee et al.*, 2004; *Wang et al.*, 2001] while under pre-seismic conditions the groundwater table remained deeper providing low base flow discharge and restricting plant transpiration to riparian vegetation due to groundwater access by deep rooting species (see Figure 10a and 10b). As the topsoil was dry during the earthquake (see Figure 2), the ascended water is likely to be absorbed by the soil matrix [*Scheffer and Schachtschabel*, 2010]. Wetting of the formerly unsaturated zone is indicated by the intensification of the diurnal streamflow oscillations (see 7.3.1). Despite the instantaneously increased hydraulic head, the flow is temporarily reduced as the expelled water saturates a portion of the formerly unsaturated zone. The temporarily reduced flow is expressed as a delayed streamflow increase at the catchments' outlets. Hence, an abrupt but transient initial decline of streamflow is expected (see insets in Figure 3), and the initial drop of streamflow discharge would continue until a new hydraulic equilibrium has been established between the saturated and unsaturated zones. Under this newly established equilibrium the rise of the water table ceases and the enlarged cross section of the lateral subsurface flow now enhances streamflow discharge following equation (4) (see Figure 10c). However, these observations are not restricted to liquefaction or undrained consolidation processes. An elevated groundwater table along the headwater valley bottoms may also be triggered by enhanced vertical permeability.

[43] The short duration of such an initial decline will not be observable at larger scales [e.g., *Manga*, 2001; *Manga et al.*, 2003; *Montgomery et al.*, 2003] because any short signals from small tributaries will be averaged over longer periods when they merge together and the discharges are superimposed. Thus, it is not surprising that the longest excess flow was sustained in Pichún grande. In the case of Pichún grande, excess flow equaled 8–9 mm until 4 May when the first significant rainfall event of the rainy season occurred, masking the streamflow response to the Maule earthquake. This value is comparable to the response of Ship Creek to the Alaska earthquake on 27 March 1960 under winter low flow conditions and limited water availability for streamflow generation [*Manga*, 2001]. Thus, the extended stream-network may explain the missing initial decline in catchments of a larger scale (see catchment No. 10 in Figures 3 and 4) but fails to explain the missing decline in catchment No. 3 and near-surface undrained consolidation may explain the hydrological response to the Maule earthquake and the lack of response to the aftershock.

7.3.1. Intensified Magnitude of Diurnal Oscillations of Streamflow Discharge

[44] Earthquakes are reported to affect whole ecosystems [*Attiwill*, 1994]. However, in this study, an enhancement in plant activity is observed, which is expressed by an intensification of diurnal oscillations of streamflow. Diurnal streamflow oscillations are governed by diurnal variability in hydraulic gradients in the unsaturated zone, as driven by the diurnal cycle of water uptake by vegetation cover which is highest during the afternoons, forcing the flux of soil water toward the roots and surface, and ceases during the night. Under these conditions, plant activity influences the amount of water available for streamflow generation and results in diurnal oscillations which are directly related to evapotranspiration and the replenishment of the depleted groundwater storage. Hence, maximum discharge occurs during the early mornings and minimum discharge during afternoons [*Dyck and Peschke*, 1995; *Gribovszki et al.*, 2010]. Thus, diurnal oscillations intensify when vegetation cover has access to additional water. Such intensified plant transpiration is documented in the increased magnitude of post-seismic diurnal oscillation in Pichún (Figure 4). Water expelled by undrained consolidation would augment the vertical extent of the capillary fringe and the saturated zone, which would facilitate root access and thus higher plant water consumption. However, a local water table rise along the headwater valley bottoms due to enhanced vertical permeability (see 7.2) could produce a similar effect.

[45] Because groundwater is ~150–200 cm below ground surface along hillslope transects, during the dry season due to sparse rainfall and high water consumption [*Huber et al.*, 2010] groundwater access is restricted to deep-rooting species along the riparian buffer strips (Figure 10c). Assuming unrestricted plant access to groundwater, streamflow discharge of all catchments (except the clear-cuts) should show at least some diurnal oscillation in streamflow. It is therefore not surprising to find diurnal streamflow oscillations in Pichún, which has the largest spatial extent of the riparian buffer zone (catchment No. 11; see Table 1). Here, the magnitude of diurnal oscillations decreased over time due to the depletion of groundwater by evapotranspiration, lack of rainfall and weather conditions which decreases potential evapotranspiration.

[46] Catchment No. 2 shows a diurnal streamflow oscillation that remained unaffected by the earthquake. As it includes a small wetland it is likely that this catchment has, in general, a groundwater table closer to the surface and thus more water available for transpiration.

7.4. Increase in Streamflow by Tilting of the Landscape?

[47] An increased $\delta h/\delta l$ due to tilting of the landscape is unlikely because it would lead either to an increased or decreased slope and some catchments should experience an increase and some a decrease in streamflow, depending on their geographical orientation. Catchments No. 9 and 11 experienced similar streamflow increases (160 and 150% respectively) but differ in their orientation whereas catchments with the same mean orientation (e.g., catchments No. 7 and 8) show high variability in relative increase (Figure 1 and Table 2). Steeper inclined slopes would also increase the surface flow velocity and thus the discharge in the streamflow, as the slope of the channel is directly related to the velocity [*Dingman*, 2002]. By analogy, enhanced vS would result in a higher discharge only for a period of the duration of the flow time in the creek. Considering a length of several 100s of meters and a flow velocity of approx. 0.2–0.4 m/s, this time is less than 1 h. The study area is close to a hinge of

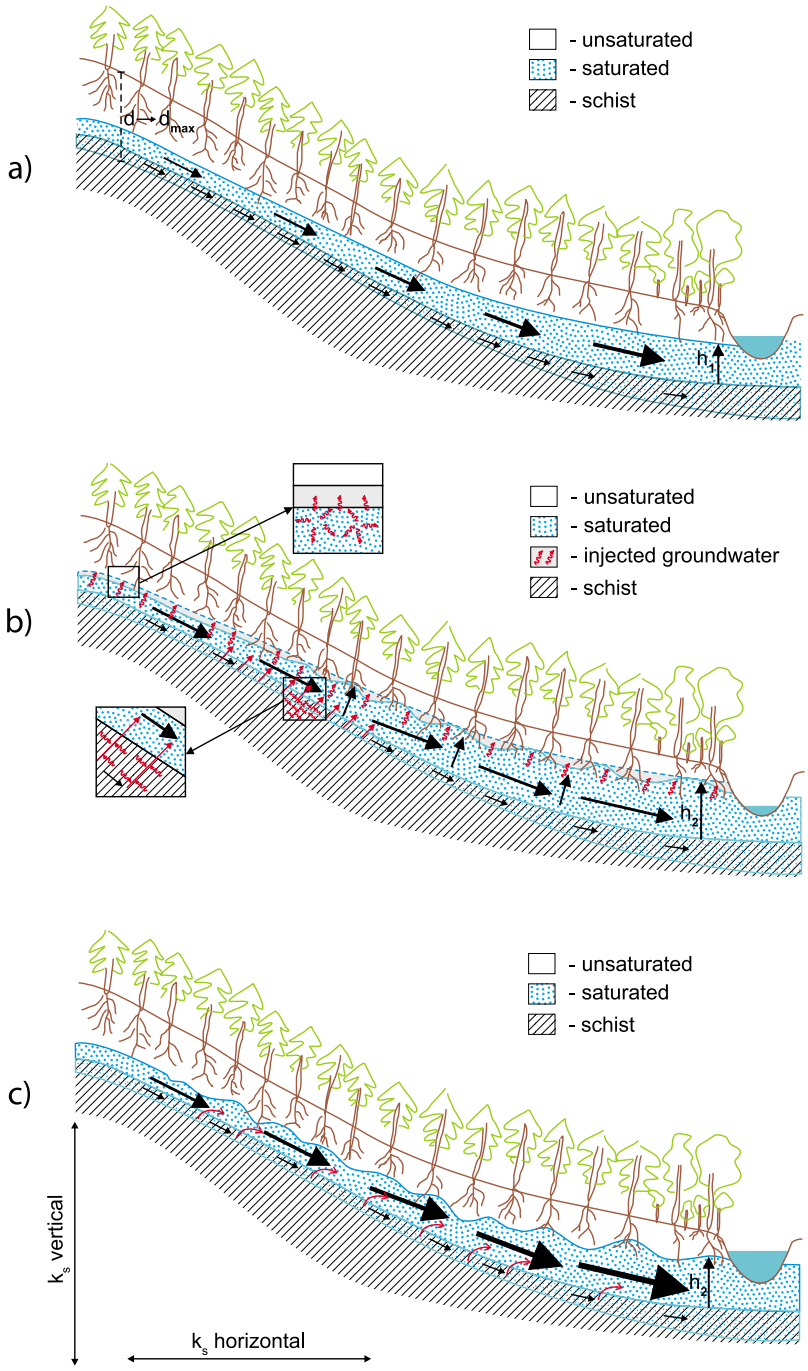

Figure 10. (a) Schematic sketch of a hillslope in the study area prior to the earthquake. The term h_1 corresponds to the height of the cross-section of saturated zone flow and d to the maximum depth of the water table. Thickness of black arrows indicates relative volume of subsurface flow and thickness of dots relative content of water in each geological unit. (b) Schematic sketch during the earthquake. The term h_2 corresponds to the vertically enlarged cross-section of the saturated zone flow. Red arrows indicate expulsion of water from fissures/cracks of the topmost schist into the saprolite layer. Rolling red arrows represent dynamic strain caused by seismic ground shaking. (c) Schematic sketch of the hillslope after the earthquake under unchanged lateral and vertical hydraulic conductivity conditions. Rolling red arrows represent additional water squeezed out from the topmost schist contributing to streamflow discharge.

vertical displacement separating the uplift area in the west from the subsidence area to the east [*Farias et al.*, 2010]. Hence, the vertical displacement is only minor compared to the lateral displacement. *Vigny et al.* [2011] showed co-seismic horizontal displacement of approx. 210 cm and vertical subsidence of ~40 cm within the study area, values similar to the land-level changes of approximately −50 cm reported by *Farias et al.* [2010] for flooded river banks of

the Bío-Bío River at ~45 km distance. However, assuming a non-uniform subsidence of approx. 0.4–0.5 m across the study area and the given altitude difference of the streams of 57 m (catchment 2) to 245 m (catchment 11) along at stream length of 400 to 2700 m (see Table 1), the possible effects on stream slope are negligible. Moreover, that subsidence is rather likely to cause retardation of streamflow discharge and high streambed roughness within the area [*Ansejo Santana*, 2011] additionally suggests attenuation of any effect of a slight modification of streambed slopes.

[48] Co-seismic streamflow discharge is highly correlated to catchment size (correlation coefficient 0.97, see section 6 for methodological details) and shows the importance of catchment scale on the pre-earthquake streamflow. Post-seismic streamflow increase is correlated to catchment size, too, which makes it very unlikely that the earthquake reshaped the extent of the drainage system. Consequently, an increased hydraulic gradient due to tilting of the landscape cannot explain the observed phenomena.

8. Conclusions and Synopsis

[49] The streamflow discharge records presented here show for the first time near-surface hydrological response to a high-magnitude earthquake in small homogeneous upland catchments. The base flow response to the main shock showed a similar but non-uniform pattern in their initial decline preceding a strong post-seismic increase and intensified diurnal streamflow oscillations. All catchments remained unaffected by the aftershock. Although minimal enhancement of lateral hydraulic conductivity was spatially limited, vertical permeability increase is probable. Substantially unchanged water temperatures show that the common source of pre- and post-seismic streamflow remained unaffected by the earthquake. Our findings indicate that the excess water originated from the saprolite-bedrock interface. Our analysis further showed that the water was released in an unequal pattern across the catchments and elevated the groundwater table which enhanced plant transpiration. Our results are consistent with the empirical magnitude-distance-relationship and the thresholds of seismic energy density needed to initiate liquefaction by undrained compaction. Although our findings allow the interpretation that undrained consolidation (perhaps even up to liquefaction) caused an initial decline followed by a subsequent post-seismic increase in streamflow discharge and intensified root water uptake, field evidence for liquefaction is lacking and enhanced vertical permeability (perhaps combined with coseismic dilatancy) provides a potential alternative explanation for the observed hydrologic response. Our results imply that further differentiation of the undrained consolidation mechanisms is crucial for understanding coseismic streamflow increases.

[50] **Acknowledgments.** The work presented herein is funded by the Chilean Government (Conicyt/BMBF 2009–092 and Fondecyt 1070218), the International Bureau of the German Ministry of Education and Research (CHL 08/03) and the Graduate School for Natural Disasters (GS NADI) of the University of Potsdam. We thank Forestry SA Mininco for access to our study catchments and financial support for the instrumentation of the catchments, Rafael Rubilar for providing soil data and Andreas Bauer for assistance with graphics (Figure 10). We thank Chi Wang, Michael Manga and Frank Krüger for constructive and helpful discussion and Alex Densmore, Simon Mudd and three anonymous reviewers for comments that significantly improved the manuscript.

References

Ansejo Santana, D. A. (2011), Transporte de sedimentos en la cuenca experimental Pichún, Región del Biobío, Chile, MS thesis, Fac. Sci. For., Univ. Austral de Chile, Valdivia, Chile.

Attiwill, P. M. (1994), The disturbance of forest ecosystems: The ecological basis for conservative management, *For. Ecol. Manage.*, *63*(2–3), 247–300, doi:10.1016/0378-1127(94)90114-7.

Bárdossy, A., and F. Schmidt (2002), GIS approach to scale issues of perimeter-based shape indices for drainage basins, *Hydrol. Sci. J.*, *47*(6), 931–942, doi:10.1080/02626660209493001.

Blume, T., E. Zehe, and A. Bronstert (2007), Rainfall-runoff response, event-based runoff coefficients and hydrograph separation, *Hydrol. Sci. J.*, *52*(5), 843–862, doi:10.1623/hysj.52.5.843.

Bosch, J. M., and J. D. Hewlett (1982), A review of catchment experiments to determine the effect of vegetation changes on water yield and evapotranspiration, *J. Hydrol.*, *55*(1–4), 3–23, doi:10.1016/0022-1694(82)90117-2.

Briggs, R. O. (1991), Effects of Loma Prieta earthquake on surface waters in Waddell Valley, *Water Resour. Bull.*, *27*(6), 991–999, doi:10.1111/j.1752-1688.1991.tb03148.x.

Brodsky, E. E., E. Roeloffs, D. Woodcock, I. Gall, and M. Manga (2003), A mechanism for sustained groundwater pressure changes induced by distant earthquakes, *J. Geophys. Res.*, *108*(B8), 2390, doi:10.1029/2002JB002321.

Carrigan, C. R., G. C. P. King, G. E. Barr, and N. E. Bixler (1991), Potential for water-table excursions induced by seismic events at Yucca Mountain, Nevada, *Geology*, *19*(12), 1157–1160, doi:10.1130/0091-7613(1991)019<1157:PFWTEI>2.3.CO;2.

Charmoille, A., O. Fabbri, J. Mudry, Y. Guglielmi, and C. Bertrand (2005), Post-seismic permeability change in a shallow fractured aquifer following a M_L 5.1 earthquake (Fourbanne karst aquifer, Jura outermost thrust unit, eastern France), *Geophys. Res. Lett.*, *32*, L18406, doi:10.1029/2005GL023859.

Dingman, S. L. (2002), *Physical Hydrology*, 646 pp., Prentice Hall, Upper Saddle River, N. J.

Dyck, S., and G. Peschke (1995), *Grundlagen der Hydrologie*, 532 pp., Verlag für Bauwesen, Berlin.

Ebel, B. A., K. Loague, D. R. Montgomery, and W. E. Dietrich (2008), Physics-based continuous simulation of long-term near-surface hydrologic response for the Coos Bay experimental catchment, *Water Resour. Res.*, *44*, W07417, doi:10.1029/2007WR006442.

Elkhoury, J. E., E. E. Brodsky, and D. C. Agnew (2006), Seismic waves increase permeability, *Nature*, *441*(7097), 1135–1138, doi:10.1038/nature04798.

Farias, M., G. Vargas, A. Tassara, S. Carretier, S. Baize, D. Melnick, and K. Bataille (2010), Land-level changes produced by the M_W 8.8 2010 Chilean earthquake, *Science*, *329*, 916, doi:10.1126/science.1192094.

Gribovszki, Z., J. Szilágyi, and P. Kalicz (2010), Diurnal fluctuations in shallow groundwater levels and streamflow rates and their interpretation: A review, *J. Hydrol.*, *385*(1–4), 371–383, doi:10.1016/j.jhydrol.2010.02.001.

Huber, A., A. Iroume, C. H. Mohr, and C. Frene (2010), Effect of Pinus radiata and Eucalyptus globulus plantations on water resource in the Coastal Range of Biobio region, Chile, *Bosque*, *31*(3), 219–230, doi:10.4067/S0717-92002010000300006.

Lee, M., T. K. Liu, K. F. Ma, and Y. M. Chang (2004), Reply to comment by N. Koizumi et al. on "Coseismic hydrological changes associated with dislocation of the September 21, 1999 Chichi earthquake, Taiwan", *Geophys. Res. Lett.*, *31*, L13604, doi:10.1029/2004GL020128.

Lorito, S., F. Romano, A. Atzori, X. Tong, A. Avallone, J. McCloskey, M. Cocco, E. Boschi, and A. Piatanesi (2011), Limited overlap between the seismic gap and coseismic slip of the great 2010 Chile earthquake, *Nat. Geosci.*, *4*(3), 173–177, doi:10.1038/ngeo1073.

Madariaga, R., M. Metois, C. Vigny, and J. Campos (2010), Central Chile finally breaks, *Science*, *328*(5975), 181–182, doi:10.1126/science.1189197.

Manga, M. (2001), Origin of postseismic streamflow changes inferred from baseflow recession and magnitude-distance relations, *Geophys. Res. Lett.*, *28*(10), 2133–2136, doi:10.1029/2000GL012481.

Manga, M., and J. C. Rowland (2009), Response of Alum Rock springs to the October 30, 2007 Alum Rock earthquake and implications for the origin of increased discharge after earthquakes, *Geofluids*, *9*(3), 237–250, doi:10.1111/j.1468-8123.2009.00250.x.

Manga, M., E. E. Brodsky, and M. Boone (2003), Response of streamflow to multiple earthquakes, *Geophys. Res. Lett.*, *30*(5), 1214, doi:10.1029/2002GL016618.

Melnick, D., B. Bookhagen, M. R. Strecker, and H. P. Echtler (2009), Segmentation of megathrust rupture zones from fore-arc deformation patterns over hundreds to millions of years, Arauco peninsula, Chile, *J. Geophys. Res.*, *114*, B01407, doi:10.1029/2008JB005788.

Mogi, K., H. Mochizuki, and Y. Kurokawa (1989), Temperature-changes in an artesian spring at Usami in the Izu Peninsula (Japan) and their relation to

earthquakes, *Tectonophysics*, *159*(1–2), 95–108, doi:10.1016/0040-1951(89)90172-8.

Montgomery, D. R., and W. E. Dietrich (2002), Runoff generation in a steep, soil-mantled landscape, *Water Resour. Res.*, *38*(9), 1168, doi:10.1029/2001WR000822.

Montgomery, D. R., and M. Manga (2003), Streamflow and water well responses to earthquakes, *Science*, *300*(5628), 2047–2049, doi:10.1126/science.1082980.

Montgomery, D. R., K. M. Schmidt, H. M. Greenberg, and W. E. Dietrich (2000), Forest clearing and regional landsliding, *Geology*, *28*(4), 311–314.

Montgomery, D. R., H. M. Greenberg, and D. T. Smith (2003), Streamflow response to the Nisqually earthquake, *Earth Planet. Sci. Lett.*, *209*(1–2), 19–28, doi:10.1016/S0012-821X(03)00074-8.

Moreno, M., M. Rosenau, and O. Oncken (2010), 2010 Maule earthquake slip correlates with pre-seismic locking of Andean subduction zone, *Nature*, *467*(7312), 198–202, doi:10.1038/nature09349.

Muir-Wood, R., and G. C. P. King (1993), Hydrological signatures of earthquake strain, *J. Geophys. Res.*, *98*(B12), 22,035–22,068, doi:10.1029/93JB02219.

Nakamura, Y., and H. Wakita (1984), Precise temperature measurement of groundwater for earthquake-prediction study, *Pure Appl. Geophys.*, *122*, 164–174.

Papadopoulos, G. A., and G. Lefkopoulos (1993), Magnitude-distance relations for liquefaction in soil from earthquakes, *Bull. Seismol. Soc. Am.*, *83*(3), 925–938.

Rawls, W. J., R. A. Lajpat, D. L. Brakensiek, and A. Shirmohammadi (1993), Infiltration and soil water movement, in *Handbook of Hydrology*, edited by D. R. Maidment, chap. 5, pp. 1–51, McGraw-Hill, New York.

Reutebuch, S., R. McGaughey, H.-E. Anderson, and W. Carson (2003), Accuracy of a high- resolution lidar terrain model under a conifer forest canopy, *Can. J. Rem. Sens.*, *29*, 527–535, doi:10.5589/m03-022.

Roeloffs, E. (1996), Poroelastic techniques in the study of earthquake-related hydrologic phenomena, *Adv. Geophys.*, *37*(37), 135–195, doi:10.1016/S0065-2687(08)60270-8.

Roeloffs, E., M. Sneed, D. L. Galloway, M. L. Sorey, C. D. Farrar, J. F. Howle, and J. Hughes (2003), Water-level changes induced by local and distant earthquakes at Long Valley caldera, California, *J. Volcanol. Geotherm. Res.*, *127*(3–4), 269–303, doi:10.1016/S0377-0273(03)00173–2.

Roelofts, E. A. (1998), Persistent water level changes in a well near Parkfield, California, due to local and distant earthquakes, *J. Geophys. Res.*, *103*(B1), 869–889, doi:10.1029/97JB02335.

Rojstaczer, S., and S. Wolf (1992), Permeability changes associated with large earthquakes - an example from Loma Prieta, *Calif. Geol.*, *20*(3), 211–214, doi:10.1130/0091-7613(1992)020<0211:PCAWLE>2.3.CO;2.

Rojstaczer, S., S. Wolf, and R. Michel (1995), Permeability enhancement in the shallow crust as a cause of earthquake-induced hydrological changes, *Nature*, *373*(6511), 237–239, doi:10.1038/373237a0.

Sato, T., H. Wakita, K. Notsu, and G. Igarashi (1992), Anomalous hot-spring water changes - possible precursors of the 1989 volcanic-eruption off the east-coast of the Izu peninsula, *Geochem. J.*, *26*(2), 73–83, doi:10.2343/geochemj.26.73.

Scheffer, F., and P. Schachtschabel (2010), *Lehrbuch der Bodenkunde*, 584 pp., Spektrum Akademischer Verlag, Berlin.

Scholz, C. H. (2010), *The Mechanics of Earthquakes and Faulting*, 471 pp., Cambridge Univ. Press, Cambridge.

Sparkes, R., F. Tilmann, N. Hovius, and J. Hillier (2010), Subducted seafloor relief stops rupture in South American great earthquakes: Implications for rupture behaviour in the 2010 Maule, Chile earthquake, *Earth Planet. Sci. Lett.*, *298*(1–2), 89–94, doi:10.1016/j.epsl.2010.07.029.

Tertulliani, A., and L. Cucci (2009), Clues to the identification of a seismogenic source from environmental effects: The case of the 1905 Calabria (Southern Italy) earthquake, *Nat. Hazards Earth Syst. Sci.*, *9*(6), 1787–1803, doi:10.5194/nhess-9-1787-2009.

Tokunaga, T. (1999), Modelling of earthquake-induced hydrological changes and possible permeability enhancement due to the 17 January 1995 Kobe Earthquake, Japan, *J. Hydrol.*, *223*(3–4), 221–229, doi:10.1016/S0022-1694(99)00124-9.

Tong, X. P., et al. (2010), The 2010 Maule, Chile earthquake: Downdip rupture limit revealed by space geodesy, *Geophys. Res. Lett.*, *37*, L24311, doi:10.1029/2010GL045805.

Vigny, C., et al. (2011), The 2010 Mw 8.8 Maule megathrust Earthquake of central Chile, monitored by GPS, *Science*, *332*(6032), 1417–1421, doi:10.1126/science.1204132.

Wang, C. Y. (2007), Liquefaction beyond the near-field, *Seismol. Res. Lett.*, *78*(5), 512–517, doi:10.1785/gssrl.78.5.512.

Wang, C. Y., and Y. P. Chia (2008), Mechanism of water level changes during earthquakes: Near field versus intermediate field, *Geophys. Res. Lett.*, *35*, L12402, doi:10.1029/2008GL034227.

Wang, C. Y., and M. Manga (2010a), *Earthquakes and Water*, 225 pp., Springer, Berlin.

Wang, C. Y., and M. Manga (2010b), Hydrologic responses to earthquakes and a general metric, *Geofluids*, *10*(1–2), 206–216, doi:10.1111/j.1468-8123.2009.00270.x.

Wang, C.-Y., and M. Manga (2012), Transient change in groundwater temperature after earthquakes, *Geology*, *40*, 119–122, doi:10.1130/G32565.1.

Wang, C. Y., L. H. Cheng, C. V. Chin, and S. B. Yu (2001), Coseismic hydrologic response of an alluvial fan to the 1999 Chi-Chi earthquake, Taiwan, *Geology*, *29*(9), 831–834, doi:10.1130/0091-7613(2001)029<0831:CHROAA>2.0.CO;2.

Wang, C. Y., C. H. Wang, and M. Manga (2004a), Coseismic release of water from mountains: Evidence from the 1999 (M_W = 7.5) Chi-Chi, Taiwan, earthquake, *Geology*, *32*(9), 769–772, doi:10.1130/G20753.1.

Wang, C. Y., M. Manga, D. Dreger, and A. Wong (2004b), Streamflow increase due to rupturing of hydrothermal reservoirs: Evidence from the 2003 San Simeon, California, Earthquake, *Geophys. Res. Lett.*, *31*, L10502, doi:10.1029/2004GL020124.

Wang, C. Y., M. Manga, C. H. Wang, and C. H. Chen (2012), Transient change in groundwater temperatures after earthquakes, *Geology*, *40*(2), 119–122, doi:10.1130/G32565.1.

Wilson, J. P., and J. C. Gallant (2000), *Terrain Analysis: Principles and Applications*, 479 pp., Wiley-Blackwell, New York.

Ziegler, A. D., J. N. Negishi, R. C. Sidle, S. Noguchi, and A. R. Nik (2006), Impacts of logging disturbance on hillslope saturated hydraulic conductivity in a tropical forest in Peninsular Malaysia, *Catena*, *67*(2), 89–104, doi:10.1016/j.catena.2006.02.008.